Acute neuroinflammation in a clinically relevant focal cortical ischemic stroke model in rat: Longitudinal positron emission tomography and immunofluorescent tracking

Tóth, Miklós[1]*; Little, Philip[1,2]*; Arnberg, Fabian[1,2,3];Häggkvist, Jenny[1];Mulder, Jan [4]; Halldin, Christer[1,5]; Gulyás, Balázs[1,5]; Holmin, Staffan[1,2]

Miklós Tóth[1*] - email: Miklos.Toth@ki.se

Philip Little[1,2*] - email: Philip.Little@ki.se

Fabian Arnberg[1,2,3]- email: Fabian.Arnberg@ki.se

Jan Mulder[4] – email: Jan.Mulder@ki.se

Jenny Häggkvist[1] - email: Jenny.Haggkvist@ki.se

Christer Halldin[1,5]- email: Christer.Halldin@ki.se

Balázs Gulyás[1,5]- email: Balazs.Gulyas@ki.se

Staffan Holmin[1,2] - email: Staffan.Holmin@ki.se

*these authors contributed equally

[1]*Karolinska Institutet, Department of Clinical Neuroscience, SE-171 76 Stockholm, SWEDEN*

[2]*Karolinska University Hospital, Department of Neuroradiology, SE-171 76 Stockholm, SWEDEN*

[3]*Karolinska University Hospital, Department of Radiology, SE-171 76 Stockholm, SWEDEN*

[4]*Science for Life Laboratory, Department of Neuroscience, Karolinska Institutet, SE-17165 Stockholm, SWEDEN*

[5]*Imperial College- NTU, Lee Kong Chian School of Medicine, Nanyang Technological University, 639798 Singapore*

Correspondence to: Miklós Tóth (miklos.toth@ki.se) and Philip Little (philip.little@ki.se)

This is the Accepted Author Manuscript of the following publication: Tóth M, Little P, Arnberg F, Häggkvist J, Mulder J, Halldin C, Gulyás B, Holmin S. Acute neuroinflammation in a clinically relevant focal cortical ischemic stroke model in rat: longitudinal positron emission tomography and immunofluorescent tracking. Brain Struct Funct. 2015 Jan 20. Doi: 10.1007/s00429-014-0970-y.

The final publication is available at link.springer.com/article/10.1007%2Fs00429-014-0970-y

Abstract

Adequate estimation of neuroinflammatory processes following ischemic stroke is essential for better understanding of disease mechanisms, and for the development of treatment strategies. With the TSPO (18 kDa Translocator Protein) PET radioligand [^{11}C]PBR28, we monitored longitudinally the inflammatory response post transient cerebral ischemia in rats, using a recently developed rat stroke model that produces isolated focal cortical infarcts with clinical relevance in size and pathophysiology. Six Sprague-Dawley rats were subjected to 90 min transient endovascular occlusion of the M2 segment of the middle cerebral artery (M2CAO). Animals were imaged with a nanoScan PET-MRI system at 1, 4, 7 and 14 days after M2CAO with a bolus injection of [^{11}C]PBR28. In the infarct region we found a significantly increased uptake of [^{11}C]PBR28 on day 4, 7 and 14 compared to day 1 as well as compared to the contralateral cortex. No significant increase was detected in the contralateral cortex during the 14 days of imaging. The activation in the infarct region gradually decreased between day 4 and day 14. In an additional group of animals (n = 26), immunofluorescence studies were performed with antibodies for activated microglia/macrophages (Cd11b, Cd68), astrocytes (GFAP) and TSPO. The TSPO immunofluorescence signal indicated reactive microgliosis post injury, corresponding to PET findings. The present clinically relevant animal model and TSPO PET ligand appear to be well suited for studies on neuroinflammation after ischemic stroke.

Key words

stroke, neuroinflammation, positron emission tomography (PET), [^{11}C]PBR28, M2CAO, rat

Introduction

Ischemic stroke is the second most common cause of mortality and morbidity worldwide, with demographic trends towards ageing population implying further increases in disability and associated health care costs over the coming decades, especially in developing countries (Donnan et al. 2008). With the emergence of new strategies for therapy of ischemic stroke, i.e. intravenous thrombolysis and mechanical thrombectomy, accurate profiling of inflammation in reperfused brain tissue is increasingly relevant (Hennerici et al. 2013; Thiel et al. 2010; Gulyás et al. 2012a,b). Understanding the inflammatory events following ischemic stroke holds bearing on assessment of potential improvements in neuroprotective and neurorestorative treatment.

Various animal models have attempted to mimic the pathophysiology of human cerebral ischemia (for review, see e.g. Cordeau and Kriz 2012; Tajiri et al. 2013; Moyanova et al. 2014). We have recently developed an endovascular method for inducing focal cortical selective occlusion of the distal segment of the middle cerebral artery (M2CAO) in the rat (Arnberg et al 2012). Comparable advantages to previously used models such as the Middle Cerebral Artery Occlusion (MCAO) model (Durukan and Tatlisumak 2007), include isolated cortical infarction with increased similarity to human stroke in relative size, preservation of pial collateral blood flow from the anterior and posterior cerebral arteries, minimal invasiveness and avoidance of hypothalamic lesions with associated alterations in water and temperature homeostasis. In addition, the present M2CAO model makes non-invasive reversal with subsequent controlled reperfusion possible, and is therefore highly suitable for longitudinal analysis of stroke pathophysiology.

Inadequate perfusion of the brain results in cerebral infarction unless blood flow is rapidly restored. Once acquired, lesions are quickly coupled with recruitment of blood born leukocytes and reactive gliosis; morphological changes in microglia and astrocytes, which are major contributors to the acute inflammatory response (Kreutzberg 1996). Acute neuroinflammation is a key component of the pathophysiological process that follows cerebral ischemia and is linked to the degree of brain damage (Raivich et al. 1999). Upon injury, microglia and astrocytes initiate structural and functional modulation that enables phagocytosis and scar formation. Activated microglia upregulate the expression of the 18 kDa translocator protein (TSPO), known previously as the peripheral benzodiazepine receptor (PBR) (Papadopoulos et al. 2006), in conjunction with morphological remodelling from ramified (resting) state, through intermediate phenotypes to the final amoeboid form (Kettenmann et al. 2011). TSPO was initially observed in microglia within and in close proximity to ischemic lesions (Myers et al. 1991; Stephenson et al. 1995) and has since also been found in reactive astrocytes encircling such regions (Rojas et al. 2007; Lavisse et al. 2012). In these cells, TSPO is upregulated to levels

significantly higher than those found in brain tissue in physiological (or resting-) conditions, which makes it suitable as target for molecular tracking of neuroinflammatory progression.

To follow the longitudinal changes in our transient focal stroke model we have selected [^{11}C]PBR28, which is a radioligand developed for TSPO imaging with positron emission tomography (PET). There are several available PET radioligands used for TSPO imaging, including [^{11}C]PK11195 (Benavides et al. 1988, Brown et al. 2007), [^{18}F]-FEPPA(Wilson et al. 2008), [^{11}C]DPA-713 and [^{11}C]DPA-714 (Chauveau et al. 2009) (for more detailed reviews, see e.g. Chauveau et al. 2008, 2009).The first radioligand developed and used for imaging microglia activation in the CNS [^{11}C]PK11195 had major drawbacks of poor signal-to-noise ratio and high non-specific binding (Guo et al. 2012). This led to the development of second generation radioligands like [^{11}C]PBR28 (Imaizumi et al. 2007, 2008). It has been shown that [^{11}C]PBR28 has low non-specific binding and increased signal-to noise ratio. These qualities makes [^{11}C]PBR28 favorable over [^{11}C]PK11195(Guo et al. 2012). [^{11}C]PBR28 has been used already to successfully visualize TSPO upregulation in non-human primates treated with LPS (Hannestad et al. 2012) and in a rat model of ischemia induced neuroinflammation (Imaizumi et al. 2007). The upregulation of TSPO has been shown several days after the induction of stroke in previous small animal experiments using the complete MCAO model. With [^{11}C]DPA-714, the highest uptake was shown at day 10 in mouse (Wang et al. 2014) and similarly at day 11 with [^{18}F]DPA-714 in rats (Martín et al. 2010). With [^{11}C]PK11195 the peak of TSPO signal was at day 7 in rats (Rojas et al. 2007), but these animals were not followed for a longer time period. For this reason we cannot exclude the possibility, that in agreement with the DPA-714 ligands, the peak uptake would come at a later timepoint.

Immunofluorescence (IF) was used to further outline the cellular response to acute ischemic injury following transient M2CAO. A triple staining regime of activated microglia and monocyte marker anti-Cd11b, along with glial fibrillary acidic protein (GFAP), was used in combination with an TSPO antibody to track acute neuroinflammation. In addition, for complete documentation of inflammatory activity within the cortical lesions produced by the M2CAO model, neuronal nuclei marker (NeuN) (Mullen et al. 1992), was used for lesion delineation, in combination with phagocyte marker anti-Cd68 in a double staining regime.

The primary objective of this study was to investigate longitudinally the acute neuroinflammatory response in a focal ischemic rat stroke model that achieves selective M2CAO and has increased clinical relevance. Longitudinal [^{11}C]PBR28 PET-imaging targeting increased TSPO expression in reactive glia and monocytes/macrophages was complemented with IF tracking of inflammatory progression.

Materials and Methods

Animals

All animal experiments were conducted according to the guidelines of the Swedish National Board of Laboratory under a protocol approved by the Ethics Review Board of Northern Stockholm, Sweden (N253/12). In our experiments 26 Sprague-Dawley (SD) rats (362 ± 28g) were used, of which six overlapped in-vivo imaging and post mortem IF analysis. Animals were housed in groups in individually ventilated cages in a thermoregulated (~ 22°C), humidity-controlled facility under a 12 h/12 h light/dark cycle with access to food and water ad libitum. After the experiments, the animals were sacrificed by decapitation under deep anesthesia.

Surgical Procedures

A heating pad with rectal thermistor was used to keep animals normothermic. Anesthesia was induced at 4% and sustained at 1.5% Isoflurane gas concentration in 100% oxygen. A 0.007F Hybrid Microwire (Balt Extrusion, Montmorency, France) sheeted within a 1.5F hydrophilic Ultraflow microcatheter (Covidien, Mansfield, MA, USA) was introduced through the ventral tail artery. An interventional angiography system (Philips AlluraXper XD, Philips Medical Systems, Best, the Netherlands) was used for navigation of the microwire tip to the M2-segment of the left middle cerebral artery creating occlusion of the artery (M2CAO). The microwire was maintained in that position for 90 minutes before withdrawal, which creates M2-segment reperfusion. Animals were allowed to recover before being returned to the animal facility. For complete surgical details see Arnberg et al 2012.

Radiochemistry and Drugs

[^{11}C]PBR28 (N-acetyl-N-(2-[^{11}C]methoxybenzyl)-2-phenoxy-5-pyridinamine) was synthesized through partial modification of a previously described method (Briard et al. 2008). In short, [^{11}C]CH_4 was released from the target and collected in a Porapak Q trap cooled with liquid nitrogen. Following collection the [^{11}C]CH_4 was released from the trap by heating with pressurized air and subsequently [^{11}C]CH_4 was mixed with vapors from iodine crystals at 60°C followed by a radical reaction occurred at 720°C. After the reaction, [^{11}C]CH_3I was collected in a Porapak Q trap at room temperature and the unreacted [^{11}C]CH_4 was recirculated for 3 min. [^{11}C]CH_3I was released from the Porapak Q trap by heating the trap using a home-produced oven to 180°C. [^{11}C]CH_3 triflate was prepared by sweeping [^{11}C]CH_3I vapour through a heated glass column containing silver-

triflate-impregnated graphitized carbon. The radiosynthesis of [^{11}C]PBR28 was obtained by trapping [^{11}C]CH_3 triflate at room temperature in a reaction vessel containing precursor desmethyl PBR28 and tetrabutylammonium hydroxide in MeOH (1.0 M, QOH) in acetone. After the reaction, the mixture was diluted with 500 µL of HPLC eluent before being injected to the HPLC system to purify [^{11}C]PBR28. The final product was isolated and formulated in phosphate buffered saline (pH = 7.4) containing less than 10% ethanol. Radiochemical purity was > 95% and specific activity at time of injection was 414 ± 239 GBq/µmol (n=23). The precursor and standard were supplied by PharmaSynth AS, Tartu, Estonia.

In vivo imaging with MRI and PET

On the experimental day (1, 4, 7 and 14 days after start of reperfusion, one animal was not imaged on day 14) the animals were anesthetized by inhalation of isoflurane (4-5% isoflurane in 100% oxygen). After induction of anesthesia, the isoflurane concentration was lowered to 1.5-2% (50/50 air/oxygen) and a cannula was inserted in the tail vein. The animals were positioned in a dedicated rat bed with hot air circulating in the bed structure to keep the animal heated and vital signs monitored continuously. All animals went through a magnetic resonance imaging (MRI) examination before each of the PET measurements. Before the start of the PET examination, the head of the animal was placed in the center of the field of view of the PET-ring. T2 weighted MRI images (FSE sequence) were collected before every PET measurement. [^{11}C]PBR28 was intravenously administered simultaneously with the start of the PET acquisition, and was followed by a 0.1 mL saline flush. The mean injected radioactivity was 17.0 ± 1.0 MBq (n = 23), the average injected mass was 0.024 ± 0.019 µg (n = 23). Upon completion of each imaging session, the animal was returned to its cage.

Imaging system and reconstruction

The PET measurements were acquired using the Mediso (Mediso Medical Imaging Systems Ltd. Budapest, Hungary) nanoScan® PET-MRI and the nanoScan® PET-CT small animal imaging systems (Szanda et al. 2011; Nagy et al. 2013). Two animals were examined at the same time in the identical PET modules of the two PET systems. The acquired list mode data was reconstructed into 25 timeframes (63 min scan = 4x10 s, 4x20 s, 4x60 s, 7x180 s, 6x360 s). The image reconstruction was made with a fully 3-dimensional penalized maximum-likelihood algorithm (MLEM; Tera-Tomo; Mediso Ltd.) with 20 iterations and without scatter or attenuation correction.

PET and MR data processing and analysis

The reconstructed dynamic PET images were co-registered to their respective, individual MRI images in PMOD (PMOD Technologies Ltd., Zurich version: 3.3). Infarct areas were defined as areas of T2 hyper intensity on day 1, while contralateral cortical areas were defined by mirroring the infarct area region to the other hemisphere. Decay corrected time activity curves (TAC) were generated. Infarct zone and contralateral cortical uptake values were expressed as percent standard uptake value (%SUV), which normalizes for injected activity and body weight (%SUV=regional activity*body weight/injected radioactivity*100). Uptake values were then calculated as a summation of uptake from 9 minutes until the end of the PET acquisition (total 54 min). Start time of this summation (at 9 minutes) was selected to remove any possible influence from the "flow phase" of imaging, where most of the signal could originate from the activity in the blood component and therefore not be directly related to TSPO activity. Statistical analyses were performed with the use of Student's two-tailed, paired t-test and statistical significance was reached when $p < 0.05$.

Immunofluorescence

Animals used for IF analysis were sacrificed at day 1, day 2, day 3, day 4, day 7, day 14 and day 22 after reperfusion. Brains were snap frozen and kept at -80°C until cryosectioned at 14µm thickness. Consecutive sections containing cortical areas located centrally in ischemic lesions were selected by macroscopic evaluation from animals sacrificed at day 1 (animal n=3), day 4 (n=4), day 7 (n=3), and day 14 (n=3). The sections were triple stained according to a standard IF protocol and tyramide signal amplification (TSA) technique (Mulder et al. 2009). Primary antibodies: Biotin conjugated anti-Cd11b, mouse monoclonal (ab33827, Abcam, Cambridge, UK), dilution 1:000; Alexa488 conjugated anti-glial fibrillary acidic protein (GFAP), mouse monoclonal (MAB3402, Cell Signaling Technology, Danvers, MA, US), dilution 1:000, and anti-TSPO (EPR5384), rabbit monoclonal (ab109497, Abcam, Cambridge, UK), dilution 1:2000. EPR5384 was validated by staining of rat and mice colon tissue as positive controls, along with negative controls omitting the primary antibody, on rat colon and brain tissue. We also performed an adsorption experiment by incubating EPR5384 antibody against TSPO (1:2000) with the C-terminal fragment of TSPO (aa156 –aa169) in a concentration of 10^{-5} for 24h prior to immunostaining. This experiment showed a clear reduction in immunofluorescence intensity.

Sections were thawed and fixated in 4% paraformaldehyde, washed in PBS, incubated with primary antibodies for 48h at 4°C and subsequently washed in TNT. TNB was used to block unspecific reactivity and sections were

then incubated for 90 minutes with secondary antibodies; Cy3 conjugated Streptavidin (Jackson Immunoresearch, West Grove, PA, USA), dilution 1:1000; horseradish peroxidase conjugated swine anti-rabbit IgG (Dako, Glostrup, Denmark), dilution 1:200, and Cy5 conjugated TSA (Perkin Elmer, Waltham, MA, USA), dilution 1:100. Hoechst (33342, Biotium Inc, Hayward, CA, USA) was used as nuclei counterstain in dilution 1:10 000.

Additional sections from lesioned brain segments were selected from animals sacrificed on day 1 (n animals =3), day 2 (n=3), day 3 (n=3), day 4 (n=3), day 7 (n=3), day 14 (n=4) and day 22 (n=3), and double stained with NeuN, rabbit polyclonal (ABN78, Millipore, Bedford, MA, USA), dilution 1:500 and anti-Cd68, mouse monoclonal (MAB1435, Millipore), dilution1:500. Sections were thawed and air dried for 30 min, fixated in 4% paraformaldehyde, washed in PBS and blocked with a mixture of 10% normal goat serum, 0.1% Triton, 0.1 Sodium Azide in PBS buffer. Tissues were subsequently incubated with primary antibodies overnight at 4°C, washed and incubated for 60 min with secondary antibodies; Cy3, goat-anti-rabbit IgG (Invitrogen, Eugene, OR, USA) 1:1000 and Alexa Fluor 488, goat-anti-mouse IgG (Invitrogen, Eugene, OR, USA) 1:500. Dapi (Sigma-Aldrich, St. Louis, MO, USA), 1: 10 000 was used as nuclear counterstain.

Image processing and semi-quantitative analysis

Cd11b/GFAP/anti-TSPO Triple staining data set: Sections were scanned with 20x primary objective initial image capture on a Vslide slide scanning microscope (Metasystems, Altlußheim, Germany) with filter sets for Dapi (EX350/50 - EM470/40), FITC (EX493/16 - EM527/30), Cy3 (EX546/10 – EM580/30), Cy3.5 (EX581/10 – EM617/40), and Cy5 (EX630/20 - 647/long pass). Initial captures were stitched in Vslide (Metasystems) software to create sectional images with microscopic resolution of relevant areas; ipsi- and contra lateral cerebral cortex extending through the corpus callosum into subcortical regions for anatomical reference. Images were analyzed in Metaviewer software (Metasystems). For confocal laser microscopy, images were captured on a Zeiss 710LSM laser-scanning microscope using z-stack multi-track consecutive channel capture configuration. Emission wavelengths for maximum separation of immunofluorescence signals were limited to 410–513 nm (Hoechst 33,342), 493–590 nm (Cy3) and 638–759 nm (Cy5). Reconstruction of GFAP+/TSPO+ and Cd11b+/TSPO+ cells was carried out by capturing consecutive images at 63× primary magnification. Three-dimensional rendering and maximum intensity projections and orthogonal images were prepared using the ZEN2011 software package (Zeiss). Images were processed and figures were assembled in CorelDraw X5 (Corel Corp., Ottawa, ON, Canada).

Primary lesion delineation was defined by absence of viable glia cells. An average area of 1.9 +/- 0.39 mm^2 were examined at 20x magnification per animal, with half of the examined area extracted from viable areas of increased GFAP expression surrounding lesion core, and the remaining half selected from areas located distally to the glial rim. NeuN/Cd68 double staining data set: sections were examined with a fluorescence microscope (Carl Zeiss AG, Jena, Germany) and a digital camera (Axiocam MRc5, Carl Zeiss AG) for image capture. Lesion delineation was performed by morphological evaluation of NeuN immunoreactive neurons, with pycnotic or otherwise ischemic appearance signifying the boundaries of the primary lesion. From within the primary lesion an area of 2.72 mm^2 per animal was examined under 40x magnification.

For both data sets, cells were registered as positive if meeting the following criteria: clear antibody immunoreactivity and positive for nuclear counterstaining. Weak or dispersed staining patterns were considered negative.

Statistical analysis

Results from each animal were normalized for size of examined tissue area and expressed as grouped averages and standard deviations. One-way ANOVA, corrected for multiple comparisons through Tukey post-hoc test, was used for calculation of statistical significance ($p< 0.05$).

Results

[^{11}C]PBR28 PET scans showed no distinguishable uptake at the infarct region one day after M2CAO compared to contralateral cortical areas, while on day 4 we detected a clearly increased uptake in the infarct region with gradual decrease at later time points (Fig. 1). These findings were corroborated by results from the temporal profile of immunofluorescent analysis (see below).

On day 1 measurements, average peak brain uptake was at 0.5 minutes (132.6 %SUV), on day 4 at 7.5 minutes (170.5 %SUV), on day 7 at 13.5 minutes (156.9 %SUV) and on day 14 at 3.5 minutes (151.4 %SUV) as can be seen in Figure 2A.

The following average %SUV values were obtained from the infarct on day 1: 67.2 ± 3.7 (n = 6), day 4: 151.2 ± 41.6 (n = 6), day 7: 141.0 ± 51.6 (n = 6); day 14: 133.0 ± 33.29 (n = 5). At day 4, 7 and 14 we found that [^{11}C]PBR28 uptake was significantly increased compared to the contralateral cortex (day 1 p =0.0512; day 4 p =0.0003, day 7 p = 0.003; day 14 p =0.0025). No significant increase was detected in the contralateral cortex region during the 14 days of imaging (Fig. 2B). The volume of the infarct region on day 1 (area of interest during all measurement days) was 20.5 ± 22.3 mm^3.

TSPO expression in activated microglia/monocytes

Cd11b and anti-TSPO antibodies were used to examine activation of microglia/monocytes in acute neuroinflammation following transient M2CAO. Results are shown in Figure 3A and Figure 4E-H, J1-3). At day 1, Cd11b positive (+) cells of circular morphology could be observed, evenly distributed throughout lesions, but with only a small fraction expressing distinguishable levels of TSPO (Fig. 4E). Total amount of Cd11b+ ($p = 0.0001$), as well as Cd11b+ cells with TSPO upregulation ($p < 0.0001$), had increased significantly by day 4. At this timepoint, Cd11b+ cells of intermediate to amoeboid morphology, expressing high levels of TSPO (Fig. 4F-G), were observed within, and adjacent to, the glial rim surrounding the lesion, and infiltrating core areas. By day 7 and day 14, total Cd11b+ cell load, although still significantly higher than on day 1 (day 7 vs. day 1 $p = 0.0013$, day 14 vs. day 1 $p = 0.0025$), decreased gradually, as did the amount of Cd11b+/TSPO+ cells (day 7 vs. day 1 $p = 0.0027$, day 14 vs. day 1 $p = 0.0436$) and the fraction of total Cd11b+ with upregulated TSPO expression. By day 14, large, morphologically irregular cells with weak Cd11b staining intensity and with marginal to undistinguishable TSPO expression were the dominating phenotype present in core areas (Fig. 4H),

whereas cells with high TSPO expression were still primarily located within or adjacent to the glial rim. Cd11b+/TSPO+ cell load was significantly lower at day 14 than at day 4 ($p = 0.0048$).

TSPO expression and reactive astrocytosis

GFAP and anti-TSPO were used to track the progress of reactive astrocytosis, surrounding the lesion core area, during the formation of glial scar tissue in the acute phase following ischemic injury (Fig. 4L). Quantifications are shown in figure 3A. On day 1, glial thinning was present along the peripheral rim surrounding core areas, with few GFAP+ cells displaying reactive morphology and TSPO immunoreactivity. By day 4, the amount of reactive astrocytes with upregulated TSPO expression had increased, but glial scar tissue was not yet clearly distinguishable. By day 7 and day 14, a significant increase (day 7 vs. day 1$p = 0.0259$, day 14 vs. day 1 $p = 0.0285$) of GFAP+/TSPO+ reactive astrocytes was present, with glial scar tissue encapsulating infarct core regions.

Phagocytic activity

NeuN and Cd68 were used to study phagocytic activity within the ischemic lesion as delineated with NeuN (Fig. 3B and Fig. 4A-D). On day 1, a small amount of Cd68+ cells of limited phagocytic activity could be observed throughout the lesion. Cell load, as well as phagocytic activity, increased gradually over day 2, day 3 and day 4 until a significant increase was established by day 7 (day 7 vs day 1: $p = 0.002$), when an abundance of amoeboid cells could be observed disseminated across the lesion. Phagocytic activity peaked by day 14 with large, plaque-like conglomerates of intensely Cd68+ cells located primarily in core areas, and cell load significantly higher than at all previous timepoints (day 14 vs days 1-4: $p<0.0001$, day 14 vs day 7 $p=0.0012$). By day 22 phagocytic activity decreased but was still significantly higher when compared to the first four days of reperfusion (Day 22 vs. day 1 $p < 0.0001$, day 22 vs. day 2 $p = 0.0005$, day 22 vs. day 3 $p = 0.0038$, day 22 vs. day 4 $p = 0.0130$).

Discussion

Acute neuroinflammatory responses to ischemic stroke have been implicated in secondary injury progression during the initial days to weeks following incident, and is a long standing focus of interest for research on focal cerebral ischemia (Barone and Feuerstein 1999; Jin et al. 2013). In the wake of advancement in acute revascularization treatment, thorough knowledge of inflammatory dynamics in the reperfused brain is of great relevance as a therapeutic target (Lakhan et al. 2009; Shah et al. 2009). Morevover, the possibility of monitoring longitudinally the neuroinflammatory response by imaging methods in this setting is important as a read-out parameter in different treatment paradigms.

In order to understand better the pathophysiological mechanisms in the human brain following an ischemic stroke, we employed an animal model of transient focal cortical ischemia, developed specifically to increase the translational value of experimental stroke research. The selective occlusion of the M2 segment of the MCA not only reproduces the most common occlusion focus of ischemic stroke in the human brain, thereby resulting in relative lesion volumes of sizes closer to those found in clinical setting (Carmichael 2005), but also preserves pial collateral flow from the anterior- and posterior cerebral arteries, the other major arteries supplying the cerebral cortex. During episodes of cerebral ischemia, collateral blood flow is a uniquely important factor in sustaining viability in compromised tissue regions adjacent to the primary necrotic lesion; the so called ischemic penumbra (Bang et al. 2008;Albers 2013). Due to the fact that reactive gliosis is initialized first in regions adjacent to the lesion core, this methodological advantage of the present model is relevant for profiling of acute neuroinflammation in reperfused brain tissue (Ito et al. 2001; Imaizumi et al. 2007;Morrison and Filosa 2013). With the advance of molecular imaging techniques, with special regard to PET, the longitudinal monitoring of various cellular processes in and around the lesion areas, including the necrotic core region and the peri-infarct region, the ischemic penumbra, has been made possible. During recent years special attention has been paid to the dynamics of microglia activation in the peri-infarct region, as this process appears to be crucial for the recovery of brain tissue. The mechanisms underlying, and the temporal dynamics of, microglial activation in animal stroke models has been studied intensively, using both in vivo molecular imaging approaches and post mortem immunohistochemical methods.

Microglial activation starts hours after a cerebral insult when resident microglia are activated and transform into phagocytic “activated microglia” within days (Stoll et al. 1998). Already 48 to 72 h after the injury, the resident microglial population in the affected region shows an intensive proliferating activity (Denes et al. 2007). This

activation does not display identical dynamics in the ischemic core and the peri-infarct zone: activated microglia appear earlier in the boundary zone of the infarct than in the core region (Walberer et al. 2010; Martin et al. 2010, 2011). In addition to the activation of the local "resident" microglia, a robust microglial infiltration to the affected region contributes to local neuroinflammation which in the peri-infarct zone reaches its peak 48–72 h following insult (Weinstein et al. 2010). Microglial activation, as a component of neuroinflammatory progression, has been shown to have potentially long-standing consequences for reperfused brain tissue. In animal stroke models, the presence of activated microglia was demonstrated up to several months after middle cerebral artery occlusion (Cordeau et al. 2008; Ekdahl et al. 2009; Weinstein et al. 2010), indicating a long term neuroinflammatory process after stroke.

As explained, a major element of neuroinflammation is the activation of resident microglial cells. This process also includes upregulation of the TSPO (18 kD translocator protein) in the mitochondrial membrane of the glial cells. TSPO upregulation is present not only in activated microglial cells, but also in reactive astrocytes, another major component of the neuroinflammatory process.

In recent years various PET radioligands have been developed to bind to the upregulated TSPO, using different molecular families including isoquinolines, benzodiazepine-chlordiazepams, quinoline-carboxaamides, eburnanes, phenylpyrazolo-pyramidine-acetamides, oxodihydropurines and aryloxyanilides (for review, see Vas and Gulyas, 2005; Boorduin et al. 2008; Chauveau 2008, 2009;Ching et al. 2012). Of these radioligands, [^{11}C]PBR28 has proven to be an eminent radioligand for labeling TSPO (Imaizumi et al. 2007, 2008; Owen et al. 2011, 2014).

Our results with [^{11}C]PBR28 and IF analysis show significant microglia/monocyte activation between the first measurements at day 1 and the second investigation at day 4, further strengthening the evidence of early upregulation of TSPO+ glial cells in the ischemic region. Considering the aim to develop methods to longitudinally follow the longstanding neuroinflammation processes in our animal model, reliability of TSPO upregulation in the ischemic region is highly important. We were able to show a statistically significant difference between the contralateral cortex and the ischemic region also on days 7 and 14 despite the gradually decreased TSPO signal compared to day 4 and the moderate animal numbers, demonstrating the feasibility of in-vivo neuroinflammation imaging in this model for even prolonged time periods.

Previously published animal models of stroke with MCAO have shown somewhat different peak TSPO signal times compared to our M2CAO results. The MCAO animal models demonstrated a TSPO peak uptake between 7 and 11 days (Wang et al. 2014; Martín et al. 2010; Rojas et al. 2007), several days after our M2CAO model

(day 4). One reason for this could be that the M2CAO produces more isolated cortical infarction, which could affect the speed of TSPO upregulation compared to MCAO. Another reason could be that the decreased invasiveness of the M2CAO leads to a faster local neuroinflammation response. In our longitudinal experiments we have observed a delay on the peak of [^{11}C]PBR28 TAC until day 7, the peak has shifted from 0.5 min on day 1 to 13.5 minutes on day 7. These changes in the time of peak brain uptake can be related to binding site density (B_{max}), since if there are more binding sites it takes more time for a ligand to reach equilibrium, which indirectly could represent the increase in TSPO availability over time. On day 14 the peak of [^{11}C]PBR28 uptake was at 3.5 minutes demonstrating another evidence for decrease of TSPO activity.

Reactive gliosis following ischemic insults is implicated in beneficial as well as detrimental effects on brain tissue and has been described as a double edged sword that may augment injury progression; specifically, the production of pro-inflammatory mediators has been linked to the destruction of viable neurons (Barreto et al. 2011;Mabuchi et al. 2000). In this study, cells were regarded as activated microglia/monocytes if expressing both Cd11b and TSPO. Considering that Cd11b is not an exclusively specific marker for microglia, it is likely that other cell types, such as blood born macrophages or neutrophils, constitute a fraction of the Cd11b+ cells negative for TSPO. Differentiating between these cells types was beyond the scope of this study.

The increase of the number of Cd11b+/TSPO+ cells revealed a rise in microglia/monocyte activation between days 1 and 4 post- reperfusion, and a significant increase by day 4. At this stage, activated microglia/monocytes of intermediate, semi-ramified or fully amoeboid morphology with high TSPO immunoreactivity (Fig. 4F-G) were found concentrated within and adjacent to the inner boundary of the glial rim surrounding the lesion core. These results corroborate previous reports of early microglia activation in experimental models (Stoll et al. 1998;Weinstein et al. 2010). Moreover, we observed that over the course of the first 14 days of reperfusion, a dynamic profile was present where activated microglia/monocytes, as they infiltrated into core regions, were more likely to display irregular, phagocytic morphology as well as, less TSPO immunoreactivity.

For assessment of regional distribution of reactive astrocytosis relative to compromised neurons, defined as neuronal nuclei of pycnotic or otherwise pathological morphology (Eke et al. 1990), GFAP was added to sections previously stained with NeuN. On day 1, this revealed glial thinning along the outer boundary of the primary lesion, running in parallel and overlapping with pycnotic neuronal nuclei (Fig. 4A1-2). Our data shows that over the first two weeks of reperfusion, reactive astrocytosis (Fig. 4K1-2), coupled with upregulation of TSPO in GFAP+ cells is increased, resulting in the gradual formation of a barrier of compact gliosis along the outer boundary of the ischemic lesion. Further, as with microglia/monocyte activation, a dynamic profile was

present where GFAP+ cells over later timepoints looked to infiltrate core areas, gradually displaying decreased reactivity as well as decreased TSPO expression, i.e. the formation of dense glial scar tissue (Fig. 4L1-2) within the necrotic core of the lesion (Sofroniew and Vinters 2010).

Longitudinal in-vivo imaging as well as IF analysis demonstrate a peak of microglia/monocyte activation on day 4 (Fig. 2B). Our results demonstrate that in contrast to the profile of the early microglia/monocyte activation that is coupled with increased TSPO expression, overall phagocytic activity within the ischemic lesion increased up until day 14 (Fig. 4A-D), corroborating rapports of extensive removal of necrotic debris during the second week after ischemic insult (Stoll et al. 1998, Mu et al. 2011). Phagocytosis as a component of neuroinflammatory progression is made up not only by activated microglia, but also by blood-born macrophages. No attempt was made to determine the specific fractions of each cell type from the total number of Cd68+ cells. Given the disparity of the respective temporal profiles for Cd11b+/TSPO+ and Cd68+ cells, as well of regional dynamics where phagocytic activity strongly displayed central agglomeration over the second week of reperfusion, our results would seem to corroborate rapports that the peak of microglia/monocyte activation precedes large scale debridement by mononuclear phagocytes in the infarct area (Schilling et al. 2003). This can be clearly explained by the sequential nature of the two mechanisms: a neuroinflammatory response is needed to overcome the acute consequences of an ischemic insult lesion, whereas the elimination of resulting cellular debris develops later as the acute phase gradually gives way to long term remodeling of lesioned brain areas.

We conclude that the longitudinal follow up of the inflammatory response with PET using the TSPO radioligand [^{11}C]PBR28 in a clinically relevant model of transient cerebral ischemia showed a significantly upregulated TSPO related signal in and around the infarct from day 4, indicating activation of microglia. This activation gradually decreased between day 4 and day 14. Imaging results were corroborated by IF analysis, which revealed a peak of microglia/monocyte activation on day 4, and a gradual increase of reactive astrocytosis and glial scar formation encapsulating the lesion, as well as of phagocytic remodeling of lesion core areas The present animal model and method for longitudinal monitoring of TSPO activation appear to be well suited for research on neuroinflammation with increased translation value as regards to human ischemic stroke.

Acknowledgements

The research leading to these results has received funding from the European Union's Seventh Framework Programme (FP7/2007-2013, GA 278850, INMiND), Uppdrag Besegra Stroke (supported by the Swedish Heart–Lung Foundation, Karolinska Institutet, Friends of Karolinska Institutet USA and the Swedish order of St John) and Söderbergska Stiftelsen.

Disclosures

None.

References

Albers GW (2013) Impact of recanalization, reperfusion, and collateral flow on clinical efficacy. Stroke 44 (6 Suppl 1):S11-12.

Arnberg F, Lundberg J, Söderman M, Damberg P, Holmin S (2012) Image-guided method in the rat for inducing cortical or striatal infarction and for controlling cerebral blood flow under MRI. Stroke 43 (9):2437-2443.

Bang OY, Saver JL, Buck BH, Alger JR, Starkman S, Ovbiagele B, Kim D, Jahan R, Duckwiler GR, Yoon SR, Viñuela F, Liebeskind DS, Investigators UC (2008) Impact of collateral flow on tissue fate in acute ischaemic stroke. J Neurol Neurosurg Psychiatry 79 (6):625-629.

Barone FC, Feuerstein GZ (1999) Inflammatory mediators and stroke: new opportunities for novel therapeutics. J Cereb Blood Flow Metab 19 (8):819-834.

Barreto G, White RE, Ouyang Y, Xu L, Giffard RG (2011) Astrocytes: targets for neuroprotection in stroke. Cent Nerv Syst Agents Med Chem 11 (2):164-173

Benavides J, Cornu P, Dennis T, Dubois A, Hauw JJ, MacKenzie ET, Sazdovitch V, Scatton B (1988) Imaging of human brain lesions with an omega 3 site radioligand. Ann Neurol 24 (6):708-712.

Briard E, Zoghbi SS, Imaizumi M, Gourley JP, Shetty HU, Hong J, Cropley V, Fujita M, Innis RB, Pike VW (2008) Synthesis and evaluation in monkey of two sensitive 11C-labeled aryloxyanilide ligands for imaging brain peripheral benzodiazepine receptors in vivo. J Med Chem 51 (1):17-30.

Brown AK, Fujita M, Fujimura Y, Liow JS, Stabin M, Ryu YH, Imaizumi M, Hong J, Pike VW, Innis RB (2007) Radiation dosimetry and biodistribution in monkey and man of 11C-PBR28: a PET radioligand to image inflammation. J Nucl Med 48 (12):2072-2079.

Carmichael ST (2005) Rodent models of focal stroke: size, mechanism, and purpose. NeuroRx 2 (3):396-409.

Chauveau F, Boutin H, Van Camp N, Dollé F, Tavitian B. (2008) Nuclear imaging of neuroinflammation: a comprehensive review of [11C]PK11195 challengers. Eur J Nucl Med Mol Imaging. 35(12):2304-2319.

Chauveau F, Van Camp N, Dollé F, Kuhnast B, Hinnen F, Damont A, Boutin H, James M, Kassiou M, Tavitian B (2009) Comparative evaluation of the translocator protein radioligands 11C-DPA-713, 18F-DPA-714, and 11C-PK11195 in a rat model of acute neuroinflammation. J Nucl Med 50 (3):468-476.

Cordeau P, Kriz J. (2012) Real-time imaging after cerebral ischemia: model systems for visualization of inflammation and neuronal repair. Methods Enzymol. 506:117-133.

Ching AS, Kuhnast B, Damont A, Roeda D, Tavitian B, Dollé F. (2012) Current paradigm of the 18-kDa translocator protein (TSPO) as a molecular target for PET imaging in neuroinflammation and neurodegenerative diseases. Insights Imaging. 3(1):111-119.

Cordeau Jr. P. Lalancette-Hébert, M. Weng, YC, Kriz, J. (2008) Live imaging of neuroinflammation reveals sex and estrogen effects on astrocyte response to ischemic injury. Stroke, 39:935–942.

Denes A, Vidyasagar R, Feng J, Narvainen J, McColl BW, Kauppinen RA, Allan SM. (2007) Proliferating resident microglia after focal cerebral ischaemia in mice. J Cereb Blood Flow Metab. 27(12):1941-53.

Donnan GA, Fisher M, Macleod M, Davis SM (2008) Stroke. Lancet 371 (9624):1612-1623.

Durukan A, Tatlisumak T (2007) Acute ischemic stroke: overview of major experimental rodent models, pathophysiology, and therapy of focal cerebral ischemia. Pharmacol Biochem Behav 87 (1):179-197.

Eke A, Conger KA, Anderson M, Garcia JH (1990) Histologic assessment of neurons in rat models of cerebral ischemia. Stroke 21 (2):299-304

Ekdahl, CT, Kokaia, Z. Lindvall, O. (2009) Brain inflammation and adult neurogenesis: the dual role of microglia. Neuroscience, 158 (2009):1021–1029.

Gulyas B, Toth M, Vas A, Shchukin E, Kostulas K, Hillert J, Halldin C (2012) Visualising neuroinflammation in post-stroke patients: a comparative PET study with the TSPO molecular imaging biomarkers [11C]PK11195 and [11C]vinpocetine. Curr Radiopharm 5 (1):19-28

Gulyás B, Tóth M, Schain M, Airaksinen A, Vas A, Kostulas K, Lindström P, Hillert J, Halldin C (2012) Evolution of microglial activation in ischaemic core and peri-infarct regions after stroke: a PET study with the TSPO molecular imaging biomarker [11C]vinpocetine. J Neurol Sci 320 (1-2):110-117.

Guo Q, Owen DR, Rabiner EA, Turkheimer FE, Gunn RN (2012) Identifying improved TSPO PET imaging probes through biomathematics: the impact of multiple TSPO binding sites in vivo. Neuroimage 60 (2):902-910.

Hannestad J, Gallezot JD, Schafbauer T, Lim K, Kloczynski T, Morris ED, Carson RE, Ding YS, Cosgrove KP (2012) Endotoxin-induced systemic inflammation activates microglia: [^{11}C]PBR28 positron emission tomography in nonhuman primates. Neuroimage 63 (1):232-239.

Hennerici MG, Kern R, Szabo K (2013) Non-pharmacological strategies for the treatment of acute ischaemic stroke. Lancet Neurol 12 (6):572-584.

Imaizumi M, Kim HJ, Zoghbi SS, Briard E, Hong J, Musachio JL, Ruetzler C, Chuang DM, Pike VW, Innis RB, Fujita M (2007) PET imaging with [11C]PBR28 can localize and quantify upregulated peripheral benzodiazepine receptors associated with cerebral ischemia in rat. Neurosci Lett 411 (3):200-205.

Imaizumi M, Briard E, Zoghbi SS, Gourley JP, Hong J, Fujimura Y, Pike VW, Innis RB, Fujita M. (2008) Brain and whole-body imaging in nonhuman primates of [11C]PBR28, a promising PET radioligand for peripheral benzodiazepine receptors. Neuroimage. 39(3):1289-1298.

Ito D, Tanaka K, Suzuki S, Dembo T, Fukuuchi Y (2001) Enhanced expression of Iba1, ionized calcium-binding adapter molecule 1, after transient focal cerebral ischemia in rat brain. Stroke 32 (5):1208-1215

Jin R, Liu L, Zhang S, Nanda A, Li G (2013) Role of inflammation and its mediators in acute ischemic stroke. J Cardiovasc Transl Res 6 (5):834-851.

Kettenmann H, Hanisch UK, Noda M, Verkhratsky A (2011) Physiology of microglia. Physiol Rev 91 (2):461-553.

Kreutzberg GW (1996) Microglia: a sensor for pathological events in the CNS. Trends Neurosci 19 (8):312-318

Lakhan SE, Kirchgessner A, Hofer M (2009) Inflammatory mechanisms in ischemic stroke: therapeutic approaches. J Transl Med 7:97.

Lavisse S, Guillermier M, Hérard AS, Petit F, Delahaye M, Van Camp N, Ben Haim L, Lebon V, Remy P, Dollé F, Delzescaux T, Bonvento G, Hantraye P, Escartin C. (2012) Reactive astrocytes overexpress TSPO and are detected by TSPO positron emission tomography imaging. J Neurosci. 32(32):10809-10818.

Mabuchi T, Kitagawa K, Ohtsuki T, Kuwabara K, Yagita Y, Yanagihara T, Hori M, Matsumoto M (2000) Contribution of microglia/macrophages to expansion of infarction and response of oligodendrocytes after focal cerebral ischemia in rats. Stroke 31 (7):1735-1743

Martín A, Boisgard R, Thézé B, Van Camp N, Kuhnast B, Damont A, Kassiou M, Dollé F, Tavitian B. (2010) Evaluation of the PBR/TSPO radioligand [(18)F]DPA-714 in a rat model of focal cerebral ischemia. J Cereb Blood Flow Metab. 30(1):230-41.

Morrison HW, Filosa JA (2013) A quantitative spatiotemporal analysis of microglia morphology during ischemic stroke and reperfusion. J Neuroinflammation 10:4.

Moyanova SG, Dijkhuizen RM. (2014) Present status and future challenges of electroencephalography- and magnetic resonance imaging-based monitoring in preclinical models of focal cerebral ischemia. Brain Res Bull. 102:22-36.

Mu S, Ouyang L, Liu B, Qu H, Zhu Y, Li K, Lei W (2011) Relationship between inflammatory reaction and ischemic injury of caudate-putamen in rats: inflammatory reaction and brain ischemia. Anat Sci Int 86 (2):86-97. doi:10.1007/s12565-010-0091-5

Mulder J, Björling E, Jonasson K, Wernérus H, Hober S, Hökfelt T, Uhlén M (2009) Tissue profiling of the mammalian central nervous system using human antibody-based proteomics. Mol Cell Proteomics 8 (7):1612-1622.

Mullen RJ, Buck CR, Smith AM (1992) NeuN, a neuronal specific nuclear protein in vertebrates. Development 116 (1):201-211

Myers R, Manjil LG, Cullen BM, Price GW, Frackowiak RS, Cremer JE (1991) Macrophage and astrocyte populations in relation to [3H]PK 11195 binding in rat cerebral cortex following a local ischaemic lesion. J Cereb Blood Flow Metab 11 (2):314-322.

Nagy K, Tóth M, Major P, Patay G, Egri G, Häggkvist J, Varrone A, Farde L, Halldin C, Gulyás B (2013) Performance evaluation of the small-animal nanoScan PET/MRI system. J Nucl Med 54 (10):1825-1832.

Owen DR, Gunn RN, Rabiner EA, Bennacef I, Fujita M, Kreisl WC, Innis RB, Pike VW, Reynolds R, Matthews PM, Parker CA. (2011) Mixed-affinity binding in humans with 18-kDa translocator protein ligands. J Nucl Med. 52(1):24-32.

Owen DR, Guo Q, Kalk NJ, Colasanti A, Kalogiannopoulou D, Dimber R, Lewis YL, Libri V, Barletta J, Ramada-Magalhaes J, Kamalakaran A, Nutt DJ, Passchier J, Matthews PM, Gunn RN, Rabiner EA. (2014) Determination of [(11)C]PBR28 binding potential in vivo: a first human TSPO blocking study. J Cereb Blood Flow Metab. 34(6):989-994.

Papadopoulos V, Baraldi M, Guilarte TR, Knudsen TB, Lacapère JJ, Lindemann P, Norenberg MD, Nutt D, Weizman A, Zhang MR, Gavish M (2006) Translocator protein (18kDa): new nomenclature for the peripheral-type benzodiazepine receptor based on its structure and molecular function. Trends Pharmacol Sci 27 (8):402-409.

Raivich G, Bohatschek M, Kloss CU, Werner A, Jones LL, Kreutzberg GW (1999) Neuroglial activation repertoire in the injured brain: graded response, molecular mechanisms and cues to physiological function. Brain Res Brain Res Rev 30 (1):77-105

Rojas S, Martín A, Arranz MJ, Pareto D, Purroy J, Verdaguer E, Llop J, Gómez V, Gispert JD, Millán O, Chamorro A, Planas AM (2007) Imaging brain inflammation with [(11)C]PK11195 by PET and

induction of the peripheral-type benzodiazepine receptor after transient focal ischemia in rats. J Cereb Blood Flow Metab 27 (12):1975-1986.
Schilling M, Besselmann M, Leonhard C, Mueller M, Ringelstein EB, Kiefer R (2003) Microglial activation precedes and predominates over macrophage infiltration in transient focal cerebral ischemia: a study in green fluorescent protein transgenic bone marrow chimeric mice. Exp Neurol 183 (1):25-33
Shah IM, Macrae IM, Di Napoli M (2009) Neuroinflammation and neuroprotective strategies in acute ischaemic stroke - from bench to bedside. Curr Mol Med 9 (3):336-354
Sofroniew MV, Vinters HV (2010) Astrocytes: biology and pathology. Acta Neuropathol 119 (1):7-35.
Stephenson DT, Schober DA, Smalstig EB, Mincy RE, Gehlert DR, Clemens JA (1995) Peripheral benzodiazepine receptors are colocalized with activated microglia following transient global forebrain ischemia in the rat. J Neurosci 15 (7 Pt 2):5263-5274
Stoll G, Jander S, Schroeter M (1998) Inflammation and glial responses in ischemic brain lesions. Prog Neurobiol 56 (2):149-171
Szanda I, Mackewn J, Patay G, Major P, Sunassee K, Mullen GE, Nemeth G, Haemisch Y, Blower PJ, Marsden PK (2011) National Electrical Manufacturers Association NU-4 performance evaluation of the PET component of the NanoPET/CT preclinical PET/CT scanner. J Nucl Med 52 (11):1741-1747.
Tajiri N, Dailey T, Metcalf C, Mosley YI, Lau T, Staples M, van Loveren H, Kim SU, Yamashima T, Yasuhara T, Date I, Kaneko Y, Borlongan CV (2013) In vivo animal stroke models: a rationale for rodent and non-human primate models. Transl Stroke Res. 4(3):308-321.
Thiel A1, Radlinska BA, Paquette C, Sidel M, Soucy JP, Schirrmacher R, Minuk J. (2010) The temporal dynamics of poststroke neuroinflammation: a longitudinal diffusion tensor imaging-guided PET study with 11C-PK11195 in acute subcortical stroke. J Nucl Med. 51(9):1404-1412.
Vas A, Gulyás B. (2005) Eburnamine derivatives and the brain. Med Res Rev. 25(6):737-757,
Walberer M, Rueger MA, Simard ML, Emig B, Jander S, Fink GR, Schroeter M. (2010) Dynamics of neuroinflammation in the macrosphere model of arterio-arterial embolic focal ischemia: an approximation to human stroke patterns. Exp Transl Stroke Med. 2(1):22.
Wang Y, Yue X, Kiesewetter DO, Wang Z, Lu J, Niu G, Teng G, Chen X. (2014) [(18)F]DPA-714 PET Imaging of AMD3100 Treatment in a Mouse Model of Stroke. Mol Pharm. [Epub ahead of print]
Weinstein JR, Koerner IP, Möller T (2010) Microglia in ischemic brain injury. Future Neurol 5 (2):227-246.
Wilson AA, Garcia A, Parkes J, McCormick P, Stephenson KA, Houle S, Vasdev N (2008) Radiosynthesis and initial evaluation of [18F]-FEPPA for PET imaging of peripheral benzodiazepine receptors. Nucl Med Biol 35 (3):305-314.

Figures

Figure 1.

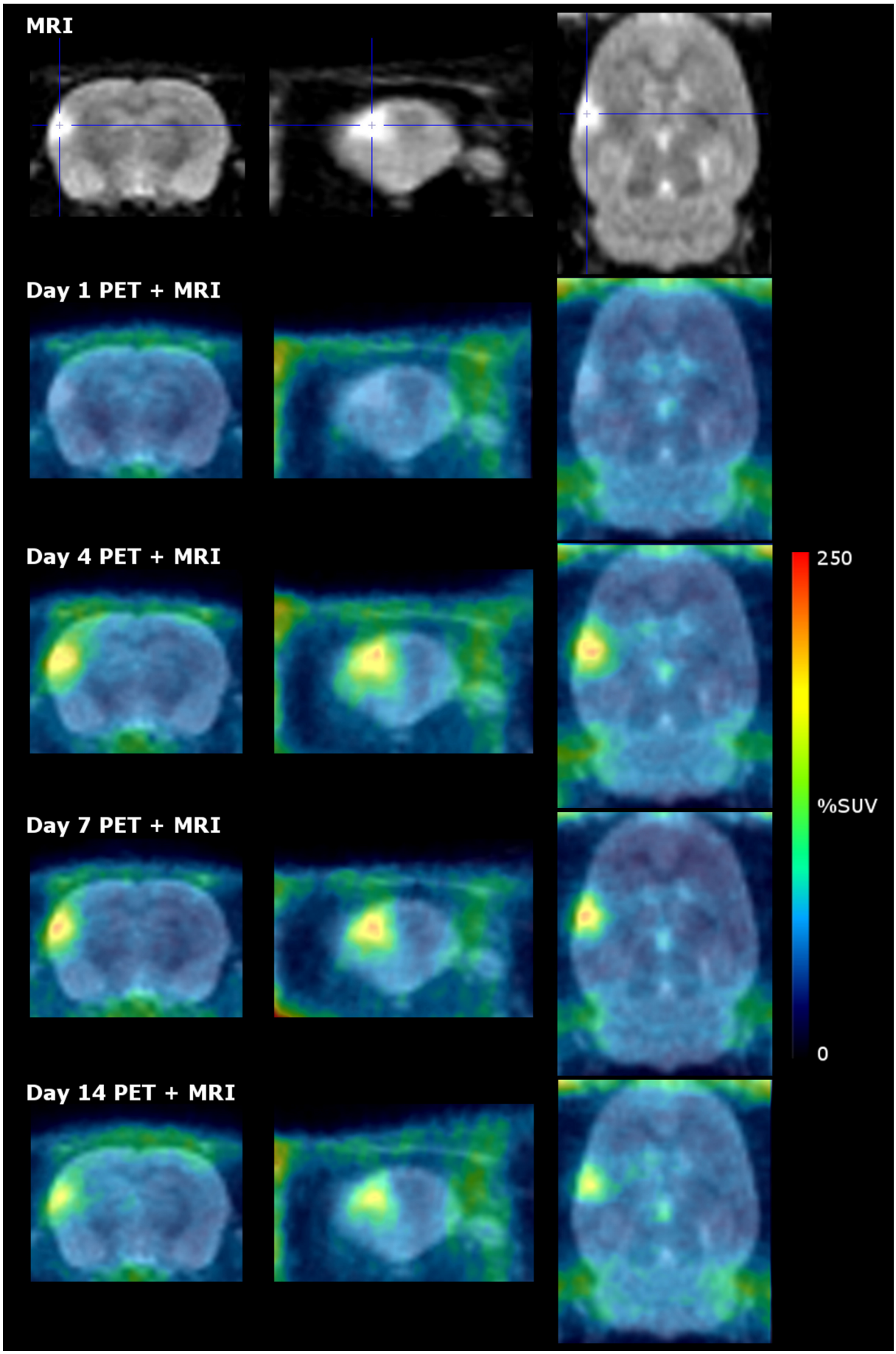
MRI
Day 1 PET + MRI
Day 4 PET + MRI
Day 7 PET + MRI
Day 14 PET + MRI
250
%SUV
0

Figure 2.

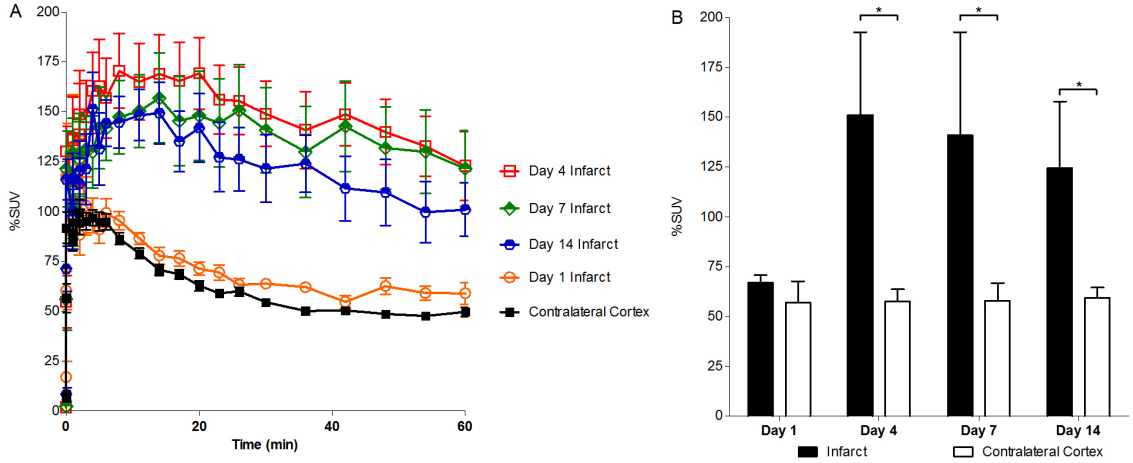
A
%SUV
Time (min)
Day 4 Infarct
Day 7 Infarct
Day 14 Infarct
Day 1 Infarct
Contralateral Cortex
B
%SUV
Day 1
Day 4
Day 7
Day 14
Infarct
Contralateral Cortex

Figure 3.

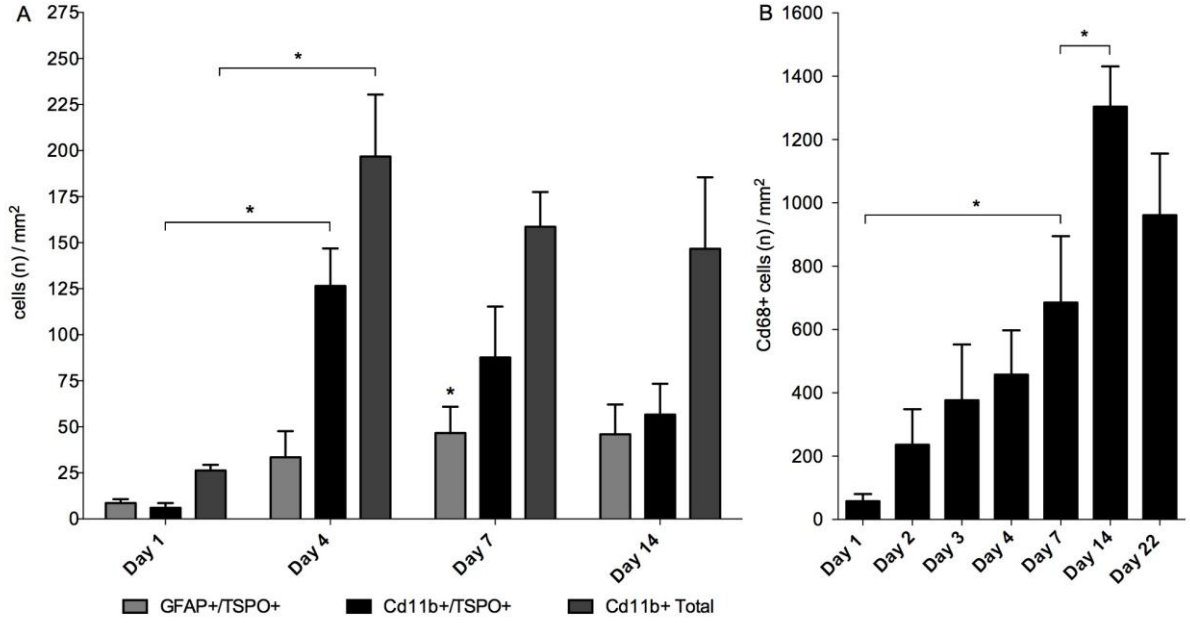
A
cells (n) / mm2
275
250
225
200
175
150
125
100
75
50
25
0
*
*
*
Day 1
Day 4
Day 7
Day 14
GFAP+/TSPO+
Cd11b+/TSPO+
Cd11b+ Total
B
Cd68+ cells (n) / mm2
1600
1400
1200
1000
800
600
400
200
0
*
*
Day 1
Day 2
Day 3
Day 4
Day 7
Day 14
Day 22

Figure 4.

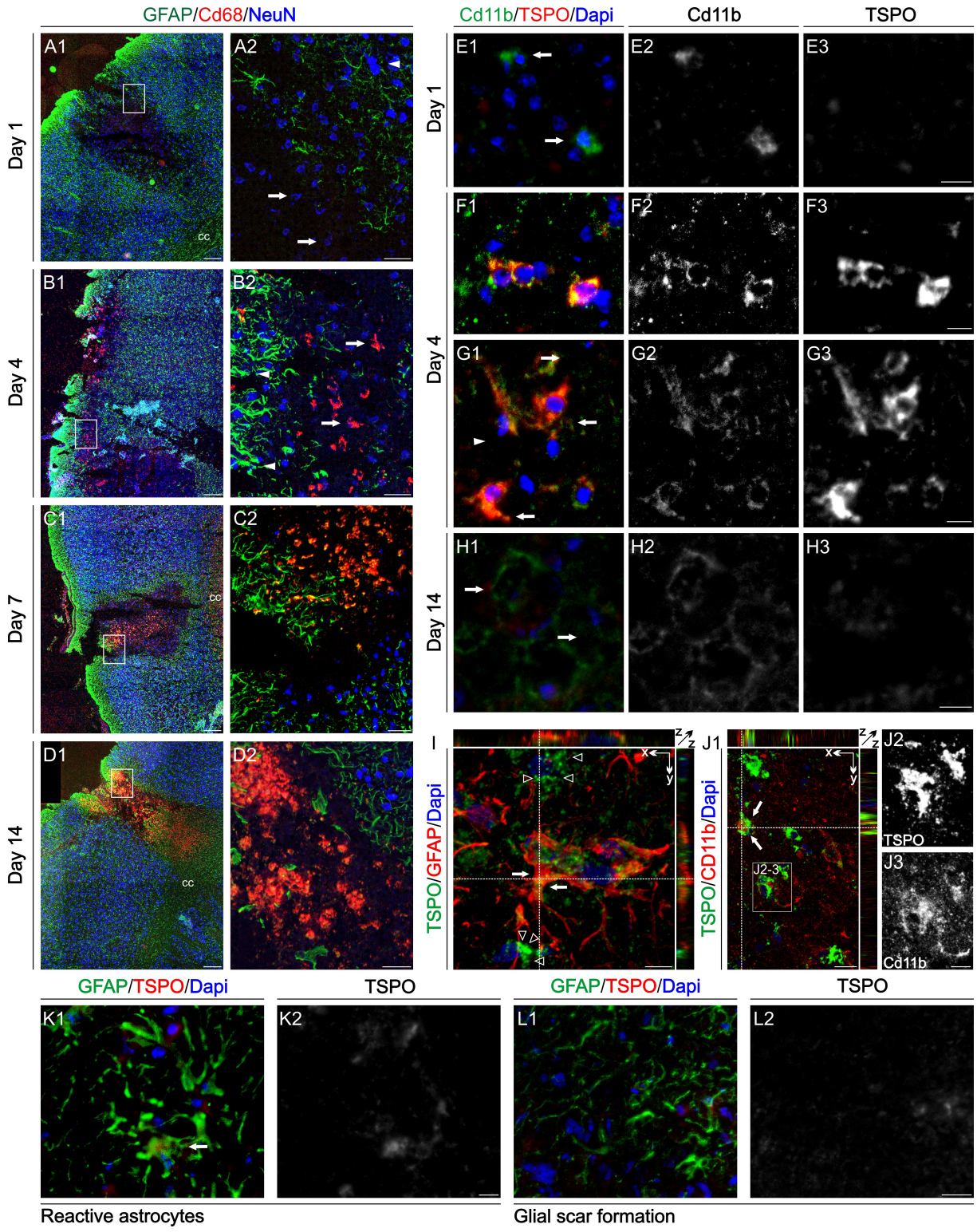
GFAP/Cd68/NeuN
Cd11b/TSPO/Dapi
Cd11b
TSPO
Day 1
Day 4
Day 7
Day 14
A1
A2
B1
B2
C1
C2
D1
D2
E1
E2
E3
F1
F2
F3
G1
G2
G3
H1
H2
H3
cc
I
J1
J2
J3
J2-3
TSPO/GFAP/Dapi
TSPO/CD11b/Dapi
TSPO
Cd11b
GFAP/TSPO/Dapi
TSPO
K1
K2
L1
L2
Reactive astrocytes
Glial scar formation

Figure Legends

Figure 1. Representative %SUV-image of [^{11}C]PBR28 uptake from day 1 to day 14 overlaid on the average of all T2 MRI scans taken from the same animal on the different days.

Figure 2. A: Average time activity curves of infarct areas on day 1(n = 6), day 4 (n = 6), day 7 (n = 6) and day 14 (n = 5) and contralateral cortical areas from all imaging days (n = 23) in %SUV B: %SUV values of [^{11}C]PBR28 uptake in the Infarct and the Contralateral Cortex region on day 1 (n = 6), day 4 (n = 6), day 7 (n = 6) and day14 (n = 5) (* = $p < 0.05$). Data expressed as mean ± SD.

Figure 3.A: Progression of GFAP+/TSPO+, Cd11b+/TSPO+ and Cd11b+ (total) cell load, from regions of reactive gliosis day 1 to day 14. B: Cd68+ phagocytic activity within the ischemic lesion at day 1 to day 22. Data presented as grouped averages of cells (n) with standard deviation and normalized for size of examined tissue. * = Significant differences ($p < 0.05$) of particular interest.

Figure 4. A-D: Phagocytic (Cd68+) and glial activity (GFAP+) 1-14 days since start of reperfusion. A1: Day 1: Glial thinning at edges of lesion core. A2: Neuronal nuclei (NeuN+) of pathological morphology (arrows) visible distally to healthy tissue (arrowhead). B1: Day 4, amoeboid phagocytes present throughout lesion. B2: Phagocytes interacting with pathological neuronal nuclei (arrows). Reactive astrocytosis is present in glial rim (arrowheads). C1-2: Day 7, increased phagocytic activity and central agglomeration. Dense, glial scar tissue now surrounds lesion core areas. D1-2: 14 days. Plaque-like clusters of phagocytes are present in core areas. Glial scar tissue is visible in the medial part of the lesion. E1-J2: TSPO upregulation in microglia (Cd11b) and astrocytes (GFAP+). E1-3: Rounded cells without TSPO expression present throughout lesion at day 1. F1-G3: Cd11b+ cells displaying morphology of intermediate (arrowhead) to amoeboid monocytes/microglia (arrows) expressing elevated levels of TSPO. These cells were located in core areas, adjacent to glial rim at 4 days since start of reperfusion. H1-3: Large macrophages/microglia with low TSPO expression located throughout the lesion core areas at 14 days after reperfusion. I-J: Reconstructed confocal laser scanned micrographs at 4 days after reperfusion: I: Demonstration of GFAP+/TSPO+ colocalisation in reactive astrocyte (closed arrows). Open arrowheads: TSPO expression in cells negative for GFAP. J1-3: Cd11b+/TSPO+ colocalisation in activated microglia/monocyte (closed arrows). K1-2: Reactive astrocytes expressing TSPO at edge of core area on day 4.

L1-2: Dense glial scar tissue from day 7 since start of reperfusion. Scale bars A1, B1, C1, D1: 200µm, A2, B2, C2, D2: 40 µm, E-I, J2-3, K1-2,: 10µm J1, L1-2: 20µm.